Production of ^{287,288}Mc isotopes in the ^{48}Ca + ^{243}Am reaction at China Accelerator Facility for Superheavy Elements

X. Y. Huang(黄鑫源)[1,2,3], Z. Y. Zhang(张志远)[1,2*], J. G. Wang(王建国)[1], L. Ma(马龙)[1,4], C. L. Yang(杨春莉)[1], M. H. Huang(黄明辉)[1,2,4], X. L. Wu(吴晓蕾)[1,4], Z. G. Gan(甘再国)[1,2,4*], H. B. Yang(杨华彬)[1,2], M. M. Zhang(张明明)[1,3], Y. L. Tian(田玉林)[1,4], Y. S. Wang(王永生)[1,4], J. Y. Wang(王均英)[1,4], Y. H. Qiang(强赟华)[1], G. Xie(谢港)[1,2], S. Y. Xu(徐苏扬)[1,2], Z. Zhao(赵圳)[1,2], Z. C. Li(李宗池)[1,2], L. C. Sun(孙路冲)[1,5], L. Zhu(祝霖)[1,2], X. Zhang(张旭)[1,2], H. Zhou(周浩)[1,2], F. Guan(管芳)[1,5], Z. H. Li(李泽浩)[1], W. X. Huang(黄文学)[1,2,4], Z. Qin(秦芝)[1], Y. Wang(王洋)[1], X. J. Yin(殷小杰)[1], Y. F. Cui(崔云飞)[1,2], Z. W. Lu(卢子伟)[1], Y. He(何源)[1,2], L. T. Sun(孙良亭)[1,2], Z. Z. Ren(任中洲)[6], S. G. Zhou(周善贵)[2,7], V. K. Utyonkov[3], A. A. Voinov[3], Yu. S. Tsyganov[3], A. N. Polyakov[3], D. I. Solovyev[3], N. D. Kovrizhnykh[3], and M. V. Shumeiko[3]

[1]*State Key Laboratory of Heavy Ion Science and Technology, Institute of Modern Physics, Chinese Academy of Sciences, Lanzhou 730000, China*
[2]*School of Nuclear Science and Technology, University of Chinese Academy of Sciences, Beijing 100049, China*
[3]*Joint Institute for Nuclear Research, RU-141980 Dubna, Russian Federation*
[4]*Advanced Energy Science and Technology Guangdong Laboratory, Huizhou 516000, China*
[5]*Department of Physics, Guangxi Normal University, Guilin 541004, China*
[6]*School of Physics Science and Engineering, Tongji University, Shanghai 200092, China*
[7]*CAS Key Laboratory of Theoretical Physics, Institute of Theoretical Physics, Chinese Academy of Sciences, Beijing 100190, China*

(Received 29 September 2025; accepted manuscript online 3 December 2025)

We report the results of the experiment on synthesizing ^{287,288}Mc isotopes (Z = 115) using the fusion-evaporation reaction ^{243}Am(^{48}Ca, 4n, 3n)^{287,288}Mc at the Spectrometer for Heavy Atoms and Nuclear Structure-2 (SHANS2), a gas-filled recoil separator located at the China Accelerator Facility for Superheavy Elements (CAFE2). In total, 20 decay chains are attributed to ^{288}Mc and 1 decay chain is assigned to ^{287}Mc. The measured α-decay properties of ^{287,288}Mc as well as its descendants are consistent with the known data. No additional decay chains originating from the 2n or 5n reaction channels were detected. The excitation function of the ^{243}Am(^{48}Ca, 3n)^{288}Mc reaction was measured at the cross-section level of picobarn, which indicates the promising capability for the study of heavy and superheavy nuclei at the facility.

DOI: 10.1088/0256-307X/43/1/010101 CSTR: 32039.14.0256-307X.43.1.010101

1. Introduction. Extending the nuclear landscape and conducting a deeper investigation of the domain of superheavy nuclei (SHN) are at the frontier of current nuclear physics research. Over the decades, cold and hot fusion reactions have been successfully employed for synthesizing heavy and superheavy nuclei,[1–3] and the seventh period of the periodic table has been completed. Despite having synthesized nuclei as heavy as ^{294}Og (Z = 118),[4] the extension of the "island of stability", which was predicted by theoretical calculations,[5–7] remains extremely challenging. The synthesis of superheavy elements (SHEs) beyond Og by utilizing heavy-ion fusion reactions faces many experimental constraints such as target availability, limited beam intensities, and consequently long measurement times at cross-section levels below the picobarn scale, etc.[8–11]

Several experimental campaigns have attempted to synthesize the new SHEs with Z = 119 or 120 using the reactions of ^{50}Ti + ^{249}Bk,[11] ^{50}Ti + ^{249}Cf,[11] ^{54}Cr + ^{248}Cm,[9] ^{64}Ni + ^{238}U,[12] and ^{58}Fe + ^{244}Pu.[13] All endeavors to synthesize the new SHEs (Z > 118) have proven unsuccessful to date. In this context, a new gas-filled recoil separator, Spectrometer for Heavy Atoms and Nuclear Structure-2 (SHANS2),[14,15] was constructed as a part of CAFE2 (China Accelerator Facility for Superheavy Elements)[16,17] at the IMP-CAS (Institute of Modern Physics, Chinese Academy of Sciences). The primary scientific objective of this facility is to investigate the physical and chemical properties of superheavy elements synthesized using extremely intense heavy-ion beams, with a particular focus on actinide targets.

To study SHN and demonstrate the capability to perform experiments with picobarn-level cross sections, we selected the reaction ^{243}Am(^{48}Ca, 3n)^{288}Mc as the first SHN synthesis experiment at the SHANS2. The Mc element (Z = 115) was first synthesized at the DGFRS (FLNR,

*Corresponding authors. Email: zhangzy@impcas.ac.cn; zggan@impcas.ac.cn
© 2026 Chinese Physical Society and IOP Publishing Ltd. All rights, including for text and data mining, AI training, and similar technologies, are reserved.

Russia) in 2004.[18] The decay properties of two isotopes ^{287}Mc and ^{288}Mc and their descendants were determined. Over the past two decades, a number of experiments for the synthesis of element Mc[19–23] were performed using the ^{48}Ca beam with an energy range of 239–259 MeV at the DGFRS[24] and DGFRS-2.[25] To date, a total of five isotopes, namely $^{286–290}$Mc, have been identified.

Further experiments aimed at the detailed study of the nuclear structure of the nuclei along the ^{288}Mc decay chain were conducted at TASCA (GSI, Germany)[26] and BGS (LBNL, USA)[27] separators in 2013 and 2015, respectively. The α-X-ray and α-γ spectroscopies were reported and the decay schemes of $^{280}\mathrm{Rg} \rightarrow {}^{276}\mathrm{Mt}$ and $^{276}\mathrm{Mt} \rightarrow {}^{272}\mathrm{Bh}$ were proposed. Later on, the mass numbers of ^{288}Mc and ^{284}Nh were directly measured for the first time with the combined BGS + FIONA apparatus.[28] Furthermore, the investigation of chemical properties of Mc and its consecutive decay products also made inspiring progress.[29,30]

In this work, we report on the results of the $^{48}\mathrm{Ca} + {}^{243}\mathrm{Am}$ experiment at SHANS2, with beam energies spanning 235.0–248.4 MeV at the middle of the target layer. The excitation function for the ^{243}Am(^{48}Ca, 3n)^{288}Mc reaction was re-investigated as well.

2. Experimental Setup. A series of experiments on synthesizing Mc isotopes were conducted from 2023 to 2025 at the CAFE2. The $^{48}\mathrm{Ca}^{14+}$ heavy ions were delivered from an Electron Cyclotron Resonance Ion Source (ECRIS) and were accelerated by a Superconducting Continuous Wave Linear Accelerator (SC-CW-Linac). Multiple beam energies spanning 251–264 MeV were employed, with a cumulative beam dose of 5.56×10^{18} ^{48}Ca ions delivered to the target.

As shown in the schematic view of SHANS2 (see Fig. 1), a differential pumping system was deployed upstream of the target chamber to isolate the high-vacuum environment (better than 10^{-5} Pa) of accelerator from the helium filling region (100 Pa) of SHANS2. The beam intensity was monitored online using a Beam Position Monitor (BPM)[31] installed in this section. The BPM data was used to collect beam dose which is calibrated periodically with a Faraday cup (FC) directly upstream of the target. The total relative uncertainty of the beam dose was estimated to be 10%.

The ^{243}Am targets (99.3% isotope enrichment) were prepared on 2.22(1)-μm-thick Ti foils by electrochemical deposition. The target segments were mounted on either a small wheel (diameter: 48 mm, capacity: 4 targets) or a medium-sized wheel (diameter: 200 mm, capacity: 10 targets). The number and average total thickness of the targets assembled in the three runs are listed in Table 1. The target wheel was rotated at a speed of ∼3000 rpm, which rotates synchronously to the beam pulse structure. Additionally, a plastic scintillator with Si-PM (Silicon PhotoMultiplier) was mounted at a 45-degree angle relative to the incident beam direction. This device allows for continuous monitoring of beam intensity and target conditions by detecting elastically scattered beam particles.

The magnet system of SHANS2 is comprised of five magnets in a $\mathrm{Q_v}$-D-$\mathrm{Q_h}$-$\mathrm{Q_v}$-D configuration, where D refers to dipole magnet and Q to quadrupole magnet. The subscripts v and h of quadrupole magnets denote horizontal and vertical focusing directions, respectively.

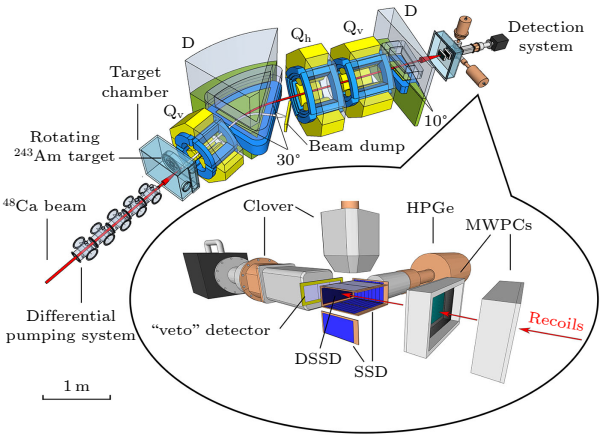

Fig. 1. Schematic view of the gas-filled recoil separator, SHANS2.[14] The detection system is composed of MWPCs, Si-Box, Veto, and germanium detectors.

Table 1. The year of run, number of used targets (N_{target}), target thickness, energy (laboratory-frame) of ^{48}Ca in the middle of the target layer, resulting excitation energy intervals (with use of mass table[32,33]), magnetic rigidity of the dipole magnets, total beam doses, number of chains assigned to ^{288}Mc (3n) and ^{287}Mc (4n), and the corresponding cross sections.

Year of run	N_{target}	Target thickness (mg/cm^2)	E_{lab} (MeV)[a]	$E^{\star}$ (MeV)[b]	$B\rho$ (Tm)	Beam dose $\times 10^{17}$	No. of chains 3n/4n	σ_{3n} (pb)	σ_{4n} (pb)
2023	4	0.57(6)[c]	241.6	33.1–36.4	2.102/2.091	8.8	5/0	$6.1^{+4.1}_{-3.0}$	
2024	10	0.48(5)[c]	240.2	32.2–34.9	2.100/2.096	3.9	4/0	$13.0^{+10.2}_{-7.1}$	
			242.7	34.2–37.0	2.093	7.8	3/1	$4.9^{+4.6}_{-3.0}$	$1.6^{+3.8}_{-1.4}$
2025	10	0.50(5)[c]	235.0	27.7–30.6	2.095	4.8	0/0	<4.7	
			238.1	30.2–33.2	2.095	6.0	3/0	$6.1^{+5.7}_{-3.7}$	
			240.2	32.0–34.9	2.095	7.3	3/0	$5.0^{+4.7}_{-3.1}$	
			244.3	35.3–38.3	2.095	8.8	2/0	$2.8^{+3.7}_{-1.9}$	
			248.4	38.9–41.7	2.095	8.2	0/0	<2.7	

[a]The beam energy was measured with a time-of-flight system, which has a systematic uncertainty of 1 MeV.
[b]The excitation energy interval represents the excitation energies of compound nuclei produced between the entrance and exit of the targets.
[c]Average ^{243}Am target thickness used for cross-section calculation.

During the experiment, The magnetic rigidity ($B\rho$) of dipole magnets were set to around 2.100 Tm (see Table 1) to center the evaporation residues (ERs) into the detection system. The deflected primary beam particles were collected by a water-cooling beam dump. The transmission efficiency of the separator was measured to be 67(11)% determined in the preparatory ^{48}Ca + ^{208}Pb reaction.

The detection system is composed of two multiwire proportional counters (MWPC), Si-Box, Veto, and germanium detectors (see zoomed view in Fig. 1). Two MWPCs filled with 300-Pa isobutane gas were mounted about 28 cm and 37 cm upstream of the stop detector (DSSD, BB17, Micron Semiconductor Ltd.), respectively. MWPC signals were later used for the tagging of events passing through the SHANS2, and distinguish them from the decays of implanted nuclei. After that, the ERs were collected by a 300-μm-thick Double-sided Silicon Strip Detector (DSSD, BB17, Micron Semiconductor Ltd.) with an active area of $48 \times 128\,\mathrm{mm}^2$. The DSSD consists of 48 horizontal strips (StripY) on the front side and 128 vertical strips (StripX) on the back side. Six Silicon Strip Detectors (SSD) were arranged perpendicular to the DSSD, forming an open box geometry (Si-Box). Each SSD has 8 strips with an active area of $120 \times 63\,\mathrm{mm}^2$. The total detection efficiency for α particles originating from the implanted nuclei was measured to be 86(8)% during the ^{48}Ca + ^{208}Pb reaction. Additionally, a 300-μm-thick segmented silicon detector (veto detector), consisting of three square-shaped segments arranged side by side, was mounted directly behind the Si-Box to register the high-energetic light particles penetrating through the DSSD.

The silicon detectors were calibrated using an external α source and the known products in the reaction ^{208}Pb(^{48}Ca, 2n)^{254}No. The energy resolution (Full Width at Half Maximum, FWHM) for 6–8 MeV α particles deposited full energy in the DSSD was ∼30 keV. The FWHM of the reconstructed α-decay events, which escaped from the DSSD and implanted in the SSD, was around ∼80 keV.

The energy calibration of the DSSD and SSD for the SF fragments with energies up to ∼200 MeV relies on the extrapolation of the calibration based on the known α decays of ^{254}No and its descendants produced in the ^{48}Ca + ^{208}Pb test reaction. The detected energy of spontaneous fission (SF) event in this work was not corrected by the pulse height defect, energy loss in the dead layers of silicon detectors, or the energy loss in the helium gas. The average total energy of fission fragments from the SF decay of ^{254}No was around 20 MeV lower than the reported total kinetic energy in Ref. [34].

In order to measure γ rays coincident with α decay or SF events, two fourfold segmented Clover detectors and one high-purity germanium detector (HPGe) were installed surrounding of the Si-Box (only for the 241.6-MeV run). Two γ sources, ^{152}Eu and ^{133}Ba, were used for the calibration of the Clover and HPGe detectors. The energy resolutions at the γ line of 356 keV (^{133}Ba) were 3–4 keV and ∼4 keV for the Clover and HPGe detector, respectively.

Ultimately, the signals from all detectors are integrated into preamplifiers and then processed in a digital data acquisition system. The 14-bit waveform digitizers [35] with a 100-MHz sampling rate were used to record samples of the input signals and transfer them to an FPGA (Field Programmable Gate Array) for real-time digital signal processing. In the FPGA, the digital RC-CR^2 and the trapezoidal filters [36,37] converted the exponential signal into a bipolar RC-CR^2 signal and a trapezoidal signal, respectively. With the energy threshold of ∼150 keV, a 30-μs-long trace from the StripX and a 20-μs-long trace from the StripY in the DSSD were recorded. Note that each StripY signal of the DSSD was simultaneously recorded by two waveform digitizers, covering energy ranges of 0.15–120 MeV and 0.5–220 MeV, respectively. Events with energies exceeding 600 keV were registered in the SSD without recording trace. To reduce noise interference and leakage current, the Si-Box and preamplifiers were cooled down to −20 ℃ and 2 ℃ using circulating alcohol, respectively.

3. Results and Discussion. We searched for genetically correlated decay chains in the same strip number and different time intervals between ER-, α-, and SF-like events. The candidates identified through correlation analysis were further examined with the inspection of the shape (trace) of the signal for each event. Additionally, the type of α-decay events was divided into five cases: (i) the event was only detected by the DSSD (full-energy event); (ii) the event was detected by both the DSSD and SSD (reconstructed event); (iii) the particle escaped from the DSSD, leaving partial energy in it, but did not enter the SSD (escaping event); (iv) the particle escaped from the DSSD, leaving the partial energy lower than the 150-keV threshold, and stopped in the SSD (escaping event); (v) the particle escaped from the DSSD, leaving the partial energy lower than the 150-keV threshold, and did not enter the SSD (missing event).

The typical counting rates, for example in the 241.6-MeV run, of the ER-like events (E = 3–20 MeV) and α-like events (E = 5–12 MeV) were ≈7.4 Hz and ≈0.3 Hz at beam intensity ≈0.5 μA on the target, respectively. Without any constraint conditions, the total counting rate across all strips of the DSSD was ≈20.5 Hz. Given the low counting rate described above, beam interruptions triggered by ER-α-α decay mode to await subsequent α-decay events were not implemented in our experiments.

The measured energy spectra shown in Fig. 2(a), obtained during the 241.6-MeV run, can be used to assess the background level under specific conditional constraints. The α-like spectrum consists of the events anti-coincident with the MWPC and veto signals. Additionally, the background of α-like events can be further suppressed by correlating with ERs within a 2-s search time window. Several peaks originating from Th, Fr, Rn, At, and Po isotopes in the region of E_α = 6–8 MeV were observed, which were produced in transfer reactions.

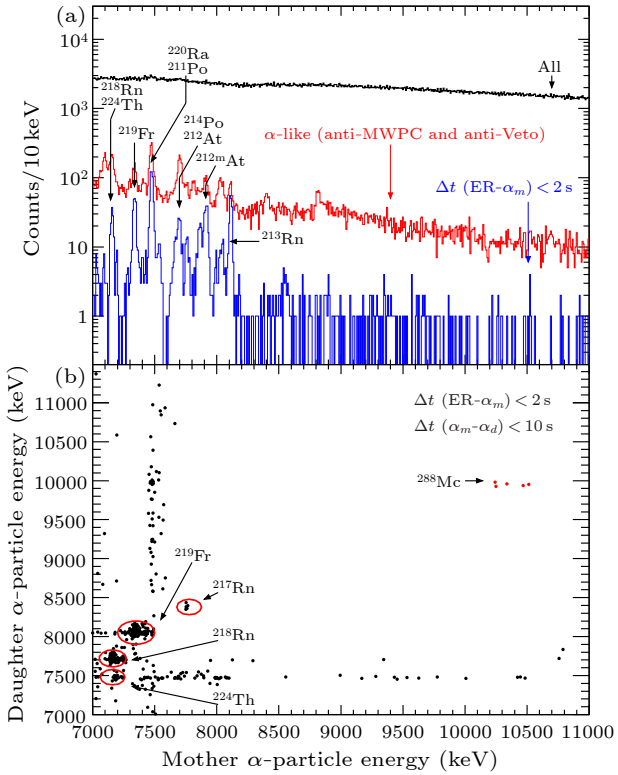

Fig. 2. (a) Energy spectra in the 241.6-MeV run. All events, α-like (anti-MWPC and anti-Veto) events, and α-like events correlated with the implantation within 2 s are shown in black, red, and blue curves, respectively. (b) Two-dimensional plot of detected mother and daughter α-particle energies for ER-α_m-α_d correlations in the 241.6-MeV run. The drawn correlated events include full-energy [case (i)] and reconstructed events [case (ii)]. The observed five ER-α(^{288}Mc)-α(^{284}Nh)-decay chains are shown in red dots.

Regarding the long α-decay chains from Mc isotopes, a search for time- and position-correlated ER-5αs-SF sequence was conducted using

- $5.0 < E_{\rm imp} < 30.0$ MeV, beam on;
- $9.5 < E_{\alpha1} < 12.0$ MeV, $\Delta t_{{\rm imp}-\alpha1} < 2$ s, or $E_{\rm SF} > 50$ MeV, $\Delta t_{{\rm imp}-{\rm SF}} < 2$ s;
- $9.0 < E_{\alpha2} < 11.5$ MeV, $\Delta t_{\alpha1-\alpha2} < 10$ s, or $E_{\rm SF} > 50$ MeV, $\Delta t_{\alpha1-{\rm SF}} < 10$ s;
- $8.5 < E_{\alpha3} < 11.0$ MeV, $\Delta t_{\alpha2-\alpha3} < 50$ s, or $E_{\rm SF} > 50$ MeV, $\Delta t_{\alpha2-{\rm SF}} < 50$ s;
- $8.5 < E_{\alpha4} < 11.0$ MeV, $\Delta t_{\alpha3-\alpha4} < 50$ s, or $E_{\rm SF} > 50$ MeV, $\Delta t_{\alpha3-{\rm SF}} < 50$ s;
- $8.0 < E_{\alpha5} < 10.0$ MeV, $\Delta t_{\alpha4-\alpha5} < 100$ s, or $E_{\rm SF} > 50$ MeV, $\Delta t_{\alpha4-{\rm SF}} < 100$ s;
- $E_{\rm SF} > 50$ MeV, $\Delta t_{\alpha5-{\rm SF}} < 100$ h.

Consequently, five searched decay chains, during the 241.6-MeV run, originating from ^{288}Mc are clearly visible. The correlations between the mother (^{288}Mc) and daughter nuclei (^{284}Nh) are highlighted by red dots in Fig. 2(b). The probability of observing random correlations with five α-decay events forming a decay chain in the 241.6-MeV run, within the α-particle energy range E_α = 5–12 MeV, was estimated to be 5.9×10^{-13} according to the method in Ref. [38].

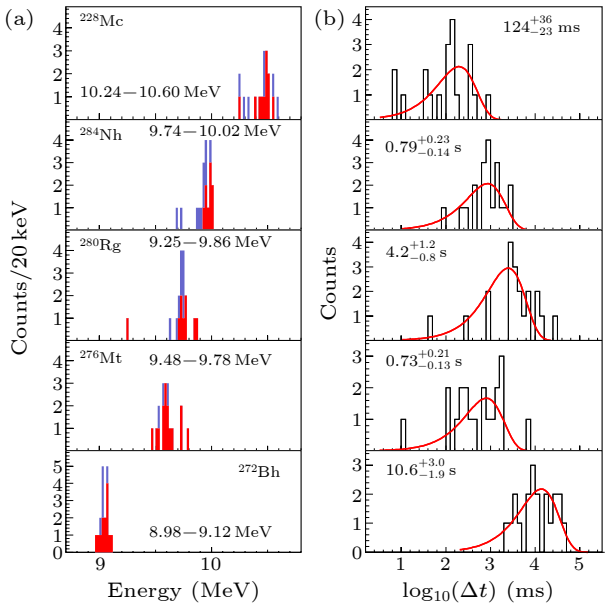

Fig. 3. (a) α-particle energy spectra, and (b) decay-time distributions on a logarithmic scale for the observed ^{288}Mc and its descendant nuclei. In the panel (a), the red histograms show the observed full-energy events, while the corresponding blue histograms show the reconstructed events. The red smooth curves in panel (b) are the expected time distributions according to the corresponding half-lives extracted from this work. The calculated half-lives $T_{1/2}$ are also shown in the panel (b), which have been extracted from all measured data.

After the detailed search for subsequent decay members and comparing with the known decay properties of ^{288}Mc and its descendants, 20 decay chains from ^{288}Mc and 1 decay chain from ^{287}Mc were finally determined in all runs (see the Supplemental Material). The α energy spectra of α particles originating from ^{288}Mc observed in this work and the decay-time distributions are shown in Fig. 3. In the energy spectra, the red histograms represent full-energy events, while the blue histograms correspond to reconstructed events. Compared with the data reported in Ref. [23], the deduced half-lives of ^{284}Nh, ^{280}Rg, ^{276}Mt, and ^{272}Bh are in good agreement within the statistical uncertainties. However, the half-life of ^{288}Mc, 124^{+36}_{-23} ms, exhibits a slight deviation (less than 50%) from the literature value, 193^{+15}_{-13} ms. This deviation is presumably attributed to the limited statistics for these isotopes.

In addition, one decay chain that was attributed to the product of the 4n-evaporation channel (^{287}Mc) was detected in the 242.7-MeV run (see Fig. 4 Chain #1). In this chain, the second and third α members are incomplete which left partial energy in the DSSD and escaped out of the Si-Box [case (iii)]. Except that, the decay properties of ^{287}Mc and its descendants match well with the ^{287}Mc data reported in Ref. [23]. The production cross section for 4n-evaporation channel is $1.6^{+3.8}_{-1.4}$ pb which is consistent with the reported $\sigma_{4n} = 0.6^{+0.7}_{-0.4}$ pb at the center-of-target beam energy of 242.2 MeV.[23] The error bar in this work considered the total uncertainties of beam dose (∼10%), target thickness (∼10%), transmission efficiency of separator [67(11)%], and detection efficiency of the detector array [86(8)%].

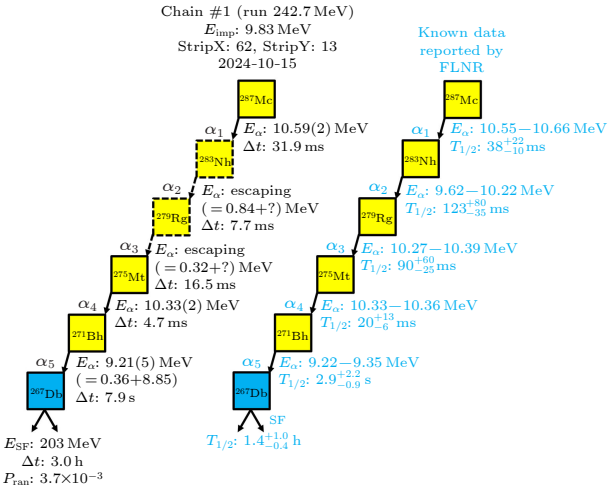

Fig. 4. The decay chain from ^{287}Mc (Chain #1). The chain is labeled with the implantation energy, strip number, and the date of registration. The energies of the reconstructed events are given as the sum of E_{DSSD} and E_{SSD} in parentheses. The random probability (P_{ran}) of the SF event for ^{287}Mc decay chain was calculated. The known decay properties of ^{287}Mc decay chains, as reported in Ref. [23], are also presented for comparison.

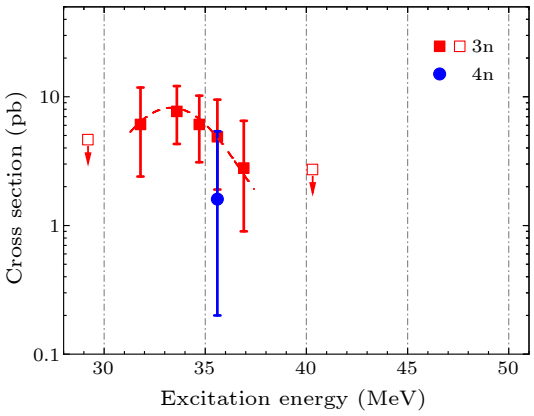

Fig. 5. Cross sections of the 3n- and 4n-evaporation channels for the ^{48}Ca + ^{243}Am reaction. Vertical error bars of the cross sections correspond to total uncertainties. The open symbols with arrows indicate the upper cross-section limits. The dashed lines through the data are drawn to guide the eye.

Figure 5 shows the excitation function of ^{243}Am(^{48}Ca, 3n)^{288}Mc reaction. Combining the beam doses of the two runs at E_{lab} = 240.2 MeV (in 2024 and 2025), the production cross section is determined to be $7.7^{+4.4}_{-3.4}$ pb. The open symbols with arrows denote the upper cross-section limits. As indicated by the dashed line, the maximum cross section for 3n evaporation channel is in the excitation energy range of 32–34 MeV. Taking into account the 1 MeV systematic uncertainty of the beam energy, the established 3n-channel excitation function agrees well with the previously reported data.[23] The measured maximum production cross section is approximately a factor of 2 lower than that reported by FLNR. This discrepancy may be attributed to the differences in the separator transmission efficiency, which was determined using a preparatory experiment with the ^{48}Ca + ^{208}Pb reaction system in this work.

No other 2n- or 5n-evaporation reaction products were observed in these experiments. The upper limits for their production cross sections were estimated to be 2–3 pb in the excitation energy range of 33–37 MeV. The further investigation of the ^{48}Ca + ^{243}Am reaction with more statistics would validate these findings more conclusively.

4. Conclusion. The synthesis of element Mc via ^{48}Ca + ^{243}Am reaction was the first attempt into the superheavy nuclei region at the SHANS2, a gas-filled recoil separator located at the CAFE2 in IMP-CAS. In total, 20 decay chains originating from ^{288}Mc and 1 decay chain from ^{287}Mc were observed, with beam energies spanning 235.0–248.4 MeV at the middle of the target layer. No additional decay chains from the 2n- or 5n-reaction channels were detected. The measured properties of ^{287,288}Mc and their daughter nuclei matched well with the existing known data. The production cross sections were determined at several projectile energies and the excitation function for the ^{243}Am(^{48}Ca, 3n)^{288}Mc reaction was measured at the picobarn cross-section level. The successful experiments at SHANS2, which utilized fusion-evaporation reactions to synthesize ^{287,288}Mc isotopes, demonstrate the capability for single atom discrimination in such challenging experiments with extremely low cross sections. From a forward-looking stance in the SHE research, this result offers a valuable reference for the future experiments on synthesizing the new elements.

Acknowledgements. The authors would like to thank the associates of the ion-source group operating the Electron Cyclotron Resonance Ion Source (ECRIS) and the colleagues obtaining ^{48}Ca beam by using Superconducting Continuous Wave Linear Accelerator (SC-CW-Linac). This work was supported in part by the National Key R&D Program of China (Contract Nos. 2023YFA1606500, 2024YFE0109800, and 2024YFE0110400), Strategic Priority Research Program of Chinese Academy of Sciences (Grant No. XDB34010000), the Gansu Key Project of Science and Technology (Grant No. 23ZDGA014), the Guangdong Major Project of Basic and Applied Basic Research (Grant No. 2021B0301030006), the National Natural Science Foundation of China (Grant Nos. 12105328, W2412040, 12475126, 12422507, 12035011, 12375118, 12435008, and W2412043), the Chinese Academy of Sciences Project for Young Scientists in Basic Research (Grant No. YSBR-002), the Youth Innovation Promotion Association of the Chinese Academy of Sciences (Grant Nos. 2020409 and 2023439), the Russian Science Foundation (Grant No. 25-42-00003).

References

[1] Münzenberg G 2015 *Nucl. Phys. A* **944** 5
[2] Morita K 2015 *Nucl. Phys. A* **944** 30
[3] Oganessian Yu Ts and Utyonkov V K 2015 *Rep. Prog. Phys.* **78** 036301
[4] Oganessian Yu Ts, Utyonkov V K, Lobanov Y V *et al.* 2006 *Phys. Rev. C* **74** 044602
[5] Meldner H 1969 *Phys. Rev.* **178** 1815

[6] Sobiczewski A, Gareev F, and Kalinkin B 1966 *Phys. Lett.* **22** 500
[7] Rutz K, Bender M, Bürvenich T, Schilling T, Reinhard P G, Maruhn J A, and Greiner W 1997 *Phys. Rev. C* **56** 238
[8] Roberto J, Alexander C, Boll R, Burns J, Ezold J, Felker L, Hogle S, and Rykaczewski K 2015 *Nucl. Phys. A* **944** 99
[9] Hofmann S, Heinz S, Mann R *et al.* 2016 *Eur. Phys. J. A* **52** 180
[10] Heßberger F P and Ackermann D 2017 *Eur. Phys. J. A* **53** 123
[11] Khuyagbaatar J, Yakushev A, Düllmann C E *et al.* 2020 *Phys. Rev. C* **102** 064602
[12] Hofmann S, Ackermann D, Antalic S *et al.* 2009 *GSI Scientific Report* p. 131
[13] Oganessian Yu Ts, Utyonkov V K, Lobanov Y V *et al.* 2009 *Phys. Rev. C* **79** 024603
[14] Xu S Y, Zhang Z Y, Gan Z G *et al.* 2023 *Nucl. Instrum. Methods Phys. Res. A* **1050** 168113
[15] Sheng L N, Hu Q, Jia H *et al.* 2021 *Nucl. Instrum. Methods Phys. Res. A* **1004** 165348
[16] Lu W, Ma H Y, Qian C *et al.* 2024 *Nucl. Instrum. Methods Phys. Res. A* **1062** 169207
[17] Gong L Y, Wang Z J, Dou W P *et al.* 2024 *Nucl. Instrum. Methods Phys. Res. A* **1058** 168819
[18] Oganessian Yu Ts, Utyonkoy V K, Lobanov Y V *et al.* 2004 *Phys. Rev. C* **69** 021601
[19] Oganessian Yu Ts, Utyonkov V K, Dmitriev S N *et al.* 2005 *Phys. Rev. C* **72** 034611
[20] Oganessian Yu Ts, Abdullin F S, Dmitriev S N *et al.* 2012 *Phys. Rev. Lett.* **108** 022502
[21] Oganessian Yu Ts, Abdullin F S, Dmitriev S N *et al.* 2013 *Phys. Rev. C* **87** 014302
[22] Oganessian Yu Ts, Utyonkov V K, Kovrizhnykh N D *et al.* 2022 *Phys. Rev. C* **106** L031301
[23] Oganessian Yu Ts, Utyonkov V K, Kovrizhnykh N D *et al.* 2022 *Phys. Rev. C* **106** 064306
[24] Subotic K, Oganessian Yu Ts, Utyonkov V, Lobanov Y, Abdullin F, Polyakov A, Tsyganov Y, and Ivanov O 2002 *Nucl. Instrum. Methods Phys. Res. A* **481** 71
[25] Oganessian Yu Ts, Utyonkov V K, Popeko A G *et al.* 2022 *Nucl. Instrum. Methods Phys. Res. A* **1033** 166640
[26] Rudolph D, Forsberg U, Golubev P *et al.* 2013 *Phys. Rev. Lett.* **111** 112502
[27] Gates J M, Gregorich K E, Gothe O R *et al.* 2015 *Phys. Rev. C* **92** 021301
[28] Gates J M, Pang G K, Pore J L *et al.* 2018 *Phys. Rev. Lett.* **121** 222501
[29] Dmitriev S N, Aksenov N V, Albin Y V *et al.* 2014 *Mendeleev Commun.* **24** 253
[30] Yakushev A, Khuyagbaatar J, Düllmann C E *et al.* 2024 *Front. Chem.* **12** 1474820
[31] Zhang Y, Hu X J, Jia H *et al.* 2022 *Nucl. Instrum. Methods Phys. Res. A* **1040** 167167
[32] Wang M, Huang W, Kondev F, Audi G, and Naimi S 2021 *Chin. Phys. C* **45** 030003
[33] Myers W and Swiatecki W 1996 *Nucl. Phys. A* **601** 141
[34] Wild J F, Hulet E K, Lougheed R W *et al.* 1994 *J. Alloy. Compd.* **213-214** 86
[35] V1724 and VX1724 *User manual* [Online]. Available: https://www.caen.it
[36] Guzik Z and Krakowski T 2013 *Nukleonika* **58** 333
[37] Jordanov V T and Knoll G F 1994 *Nucl. Instrum. Methods Phys. Res. A* **345** 337
[38] Schmidt K H, Sahm C C, Pielenz K, and Clerc H G 1984 *Z. Phys. A* **316** 19